Available online at www.sciencedirect.com
SCIENCE DIRECT®
International Journal of Multiphase Flow 30 (2004) 1051–1069
International Journal of Multiphase Flow
www.elsevier.com/locate/ijmulflow

Drag reduction in horizontal annular two-phase flow

R.L.J. Fernandes [a,*], B.M. Jutte [a], M.G. Rodriguez [b]

[a] *Shell Exploration and Production, Research and Development, Kessler Park 1, P.O. Box 60, 2280 AB Rijswijk, The Netherlands*

[b] *Department of Mechanical Engineering, University of Alberta, Edmonton, Alta., T6G 2G8 Canada*

Received 20 November 2003; received in revised form 18 May 2004

Abstract

Experiments of drag reduction in a horizontal, two-phase, annular flow are presented. The experiments were conducted in a high-pressure gas-condensate flow in 19 mm diameter pipe. The drag reducers were high molecular weight poly-alpha-olefin polymers. Motivated by the results of flow visualization, a model was developed which accounted for the drag reduction as a reduction of the height of the short-wavelength waves on the liquid film, and a reduction of the entrainment rate of droplets from the liquid film into the gas core. There was a reasonable quantitative agreement between the model predictions and the present experimental data. The model was also found to be equally effective when applied to drag reduction experiments in air–water annular flow from the literature. It properly account for the variation of drag reduction with superficial liquid velocity, superficial gas velocity, and pipe diameter.

Keywords: Multiphase drag reduction; Annular flow; Horizontal gas–liquid flow; Gas-condensate flow; Entrainment; Interfacial friction

1. Introduction

In multiphase production systems, the distance from the wellhead to the gas–liquid separator is typically about 10–30 km, but can be as much as 100 km. A high-pressure drop due to multiphase effects in these pipelines often imposes a significant back pressure on the wells and reduces their production rate. This study is motivated by the desire to apply drag reducers as a means of

* Corresponding author.
E-mail address: richard.fernandes@shell.com (R.L.J. Fernandes).

0301-9322/$ - see front matter
doi:10.1016/j.ijmultiphaseflow.2004.05.011

reducing the pressure drop in multiphase pipelines, and thereby increase the production rate in multiphase production systems.

Particularly problematic are gas-condensate production systems that operate in the annular flow regime. Due to the high gas velocities associated with annular flows (superficial gas velocities typically between 5 and 20 m/s, and superficial liquid velocities typically between 0.02 and 1.0 m/s), such systems generally have very high-pressure drops. Pressure gradients are typically in the range of 0.5–4 bar/km, resulting in pressure drops typically between 20 and 80 bar.

Experimentally, it is well established that polymer drag-reducing agents (DRAs) have a significant effect on the pressure gradient in two-phase air–water annular flow (Sylvester and Brill, 1976; Al-Sarkhi and Hanratty, 2001a). Industrial applications, on the other hand, will be primarily in high-pressure multiphase flow of hydrocarbons. However, due to the difficulty of performing high-pressure flowloop experiments with highly flammable mixtures, such data are difficult to obtain and were not available. Without such data, it is not clear how to scale the results from drag reduction studies in low-pressure air–water flows to high-pressure two-phase flow of hydrocarbons. A key contribution of this study is the presentation of drag reduction experiments in a high-pressure (10 bar) gas-condensate two-phase annular flow. The comparison air–water data with the present gas-condensate data will better enable the scaling of the former (which are readily available) to field conditions (which are closely approximated by the latter). From a more practical viewpoint, the experiments tested the robustness of oil soluble DRAs (poly-alpha-olefins) under two-phase conditions very close to those in the field and found them to be effective even under the highest shear rates likely to be encountered.

A second contribution of this study is the development and validation of a generally applicable mechanistic model capable of predicting drag reduction in annular two-phase flow. Prior to this study, a model capable of predicting the drag reduction in annular flow (or other flow regimes) had not been developed. Motivated by the results of flow visualization (e.g. Al-Sarkhi and Hanratty, 2001a; Fernandes, 2003), the drag reduction was assumed to be due to the reduction of the height of short-wavelength waves on the annular liquid film (which act as roughness elements) and the reduction of the entrainment rate of droplets from the liquid film into the gas core. The model was validated against the present gas-condensate data and air–water data from the literature (Al-Sarkhi and Hanratty, 2001a,b) and was found to be applicable to both types of flow. In particular, it was able to determine the dependence of the magnitude of drag reduction as a function of U_{SL} and U_{SG}, and account for the differences in pressure and pipe diameter. The model was used to examine the mechanisms responsible for drag reduction and attempt to ascertain the relative contributions of the mechanisms to the overall drag reduction.

1.1. Literature review

The present review focuses on drag reduction in annular flow. A broader discussion of the multiphase drag reduction literature can be found in the survey by Manfield et al. (1999). They considered drag reduction by additives such as polymers, surfactants, fibres, and other types of particles. They concluded that while it is clear that DRAs are effective in multiphase flows, a fundamental understanding of the drag reduction phenomenon in such flows is still a long way off. Even with the advances in the time since their review, their conclusion is still applicable.

Sylvester and Brill (1976) conducted a study of multiphase drag reduction in an air–water two-phase flow using polyethylene oxide at 100 ppm (parts-per-million by mass of liquid). They studied the annular flow regime in a horizontal 1.27 cm diameter pipe. The highest drag reductions were observed for the highest superficial gas velocities and were approximately 35%. This contradicts the findings in the current experiments.

Kang and co-workers (e.g. Kang and Jepson, 1999, 2000; Daas et al., 2000) have studied drag reduction in horizontal or slightly inclined slug flows and annular entrained flows using oil, gas (carbon dioxide), and in some cases, a water phase. Their measurements took place in a 10 cm diameter horizontal pipe at 1.3 bar. They report drag reductions of approximately 30–50% in annular flow at DRA concentrations of 10–50 ppm of an unspecified DRA. The superficial gas velocity in their experiments was between 10 and 12 m/s. The magnitude drag reduction decreased with increasing superficial liquid velocity (U_{SL}), going from DR = 50% at $U_{SL} = 0.5$ m/s to DR = 30% at $U_{SL} = 1.0$ m/s. This also contradicts the findings in the current experiments.

Al-Sarkhi and Hanratty (2001a) conducted a detailed experimental study of drag reduction in an annular air–water two-phase flow. The experiments were conducted in a 9.53 cm diameter pipe at slightly above atmospheric pressure. In a subsequent study (Al-Sarkhi and Hanratty, 2001b), they conducted similar experiments in a 2.54 cm diameter in order to examine the effect of pipe diameter on the drag reduction. In both studies, they used a co-polymer of polyacrylamide and sodium-acrylate. The magnitude of the drag reduction increased with increasing polymer concentration until a concentration of approximately 15 ppm was reached. Beyond 15 ppm, no additional drag reduction was observed.

The used superficial gas velocities in the range $U_{SG} = 28$–52 m/s, and superficial liquid velocities in the range $U_{SL} = 0.03$–0.20 m/s. They measured drag reductions in the range of 10–63%. In general, the drag reduction increased with increasing U_{SL} and decreased with increasing U_{SG}. This result contradicts the finding of Kang and Jepson (2000) and Sylvester and Brill (1976), but is consistent with the present experiments. In general, the drag reduction was higher in the 2.54 cm pipe (maximum of 63%) than in the 9.53 cm pipe (maximum of 48%).

2. Drag reduction

The effectiveness of the polymer drag-reducing agent (DRA) in reducing the pressure gradient is denoted drag reduction (DR) and is defined as:

$$\mathrm{DR} = \frac{\Delta P - \Delta P_{\mathrm{DRA}}}{\Delta P} = 1 - \frac{\Delta P_{\mathrm{DRA}}}{\Delta P}, \tag{1}$$

where ΔP is the pressure drop with no DRA, and ΔP_{DRA} is the pressure drop with DRA present. Alternatively, drag reduction can be defined as:

$$\mathrm{DR} = 1 - \frac{f_{\mathrm{DRA}}}{f}, \tag{2}$$

where f is the friction factor with no DRA and f_{DRA} is the friction factor with DRA present. In an annular flow, following Al-Sarkhi and Hanratty (2001a), we define the two-phase friction factor as:

$$f = \frac{D}{2\rho_G U_{SG}^2}\frac{dP}{dx}, \tag{3}$$

where D is the pipe diameter, ρ_G is the gas density, and dP/dx is the pressure gradient of the multiphase flow.

The two drag reduction definitions are quantitatively equivalent when the superficial gas velocity and gas density are identical with and without the DRA. However, in the present experiment, where the pressure gradient with and without the DRA were measured simultaneously at different axial positions in the pipe (see Section 3), the gas density and superficial gas velocity changed slightly so the second equation is used.

2.1. Pressure gradient model for annular flow

The single-phase gas and liquid frictional pressure gradients are denoted $(dP/dx)_{SG}$ and $(dP/dx)_{SL}$ respectively and are defined as:

$$\left(\frac{dP}{dx}\right)_{SG} = 2f_{SG}\rho_G U_{SG}^2/D, \tag{4}$$

$$\left(\frac{dP}{dx}\right)_{SL} = 2f_{SL}\rho_L U_{SL}^2/D, \tag{5}$$

where, f_{SG} and f_{SL} are the Fanning friction factors for the single-phase flow of gas and liquid respectively, ρ_G and ρ_L are the gas and liquid density respectively.

The Lockhart-Martenelli parameter X is the square root of the ratio of the single-phase frictional pressure gradient of the liquid and gas flow and is defined as (Oliemans, 1998):

$$X = \sqrt{\frac{(dP/dx)_{SL}}{(dP/dx)_{SG}}} = \sqrt{\frac{f_{SL}}{f_{SG}}}\frac{F_{SL}}{F_{SG}}, \tag{6}$$

where F_{SL} and F_{SG} are the square roots of densimetric liquid and gas Froude numbers respectively. They are defined as:

$$F_{SL} = \sqrt{\frac{\rho_L U_{SL}^2}{\Delta\rho g D}}, \tag{7}$$

$$F_{SG} = \sqrt{\frac{\rho_G U_{SG}^2}{\Delta\rho g D}}, \tag{8}$$

where $\Delta\rho = \rho_L - \rho_G$ is the density difference between the liquid and the gas, g is the acceleration due to gravity.

In an annular flow, $X^2 \ll 1$, and $(dP/dx)_{SL} \ll dP/dx$. In the present experiments in annular flow, typically $X^2 < 0.1$ and $(dP/dx)_{SL} < 0.02\,dP/dx$. In contrast, since the superficial gas velocities were in the 10–20 m/s range, $(dP/dx)_{SG} \approx 0.2\,dP/dx$.

We argue that a low value of the parameter X^2 suggests that the turbulent processes in the liquid film have a negligible direct contribution to the pressure gradient. That is, most of the two-phase pressure gradient in annular flow is due to the gas flow and the interaction between the gas

and liquid phases. It is therefore unlikely that suppressing the turbulence in the liquid film contributes significantly to the drag reduction observed. Since the drag reducers do not enter the gas phase, they do not directly affect $(dP/dx)_{SG}$ either. We therefore assert that the drag reduction in annular flows is achieved by the suppression of the interaction between the gas and liquid phases.

The injection of DRA into a multiphase flow can induce the flow regime to change (e.g. Kang and Jepson, 1999; Al-Sarkhi and Hanratty, 2001a; Fernandes, 2003; Wilkens et al., 2003). In an annular flow, the injection of the DRA can cause the flow to transition to either:

1. Annular flow with a much smoother gas–liquid interface and very low entrainment (e.g. Al-Sarkhi and Hanratty, 2001b, present experiment), or
2. Annular flow with a smoother gas–liquid interface and more stratified appearance—i.e., a thicker film on the bottom of the pipe than on the top (present experiment), or
3. A stratified flow (the liquid film no longer wetting the entire perimeter) and virtually no entrainment (e.g. Al-Sarkhi and Hanratty, 2001a).

The polymers used in this study were high molecular weight poly-alpha-olefins—polymers or co-polymers consisting of monomers of olefins (C_nH_{2n}) with carbon numbers of 4 or more (e.g. butene C_4H_8, or hexene C_6H_{12}). These are available from several oilfield chemical suppliers (e.g. Baker Petrolite, Conoco Specialty Products, Clariant, MI Production Chemicals). The rheological properties of poly-alpha-olefins in a hydrocarbon liquid are analogous to polymers such as polyacrylamide or poly-ethylene-oxide in water. In particular, at high concentrations (e.g. 0.1% by mass or more), they impart a high shear viscosity to the solvent, and exhibit shear-thinning, viscoelastic behaviour. In dilute form (e.g. 100 ppm or lower), they do not effect the shear viscosity of the solvent but impart a high tensional viscosity. In a single-phase flow, the tensional viscosity suppresses extensional deformations that are associated with the production of turbulent kinetic energy. Similarly, in the present flow, we speculate that the polymers suppress extensional deformations that are associated with the formation of short-wavelength surface waves and the shearing off of droplets into the gas core. Indeed, drag reducers are commonly applied as a means of droplet and mist suppression (e.g. Bachman and Shih, 1994; Khatib, 1998). However, the details of how such polymers work at the micro-scale in two-phase flows is not known.

Instead, motivated by the observation of the suppression of short-wavelength waves and the droplet entrainment, we propose to model the drag reduction in an annular flow by a mechanistic model that quantifies the effect of these phenomena on the pressure gradient. Since the short-wavelength waves act as roughness elements in turbulent flow, we also use the term liquid-film roughness to describe the phenomenon.

In order to develop the model, the expression for the pressure gradient is formulated in terms of parameters that account for the entrainment and liquid-film roughness. Then the entrainment and roughness parameters are adjusted to account for the lower entrainment and liquid-film roughness. The experimental data can then be used to determine if the model captures the quantitative and qualitative features of the drag reduction in annular flow.

The present drag reduction model is valid for annular flows with $X^2 \ll 1$, and $(dP/dx)_{SL} \ll dP/dx$. These criteria are met in the present experiment, in air–water annular flows (e.g. Al-Sarkhi and Hanratty, 2001a), and in field-scale gas-condensate pipelines operating in the annular regime.

In summary, we assume that there are three main effects that contribute to the pressure gradient in an annular flow:

(1) the hydrostatic pressure gradient,
(2) the interfacial friction at the gas liquid interface, and
(3) entrainment.

For horizontal flows, the hydrostatic term vanishes and the pressure gradient is due to interfacial friction and entrainment. To model the pressure gradient (Miesen, 1994), we consider a control volume over a length of pipe L, coinciding with the annular gas–liquid interface as shown in Fig. 1. The flow is assumed to be fully developed and statistically steady. The pipe diameter is denoted D and the liquid film has an average thickness denoted d. The superficial velocity of liquid film is denoted U_{SLf}, the superficial velocity of the entrained liquid is denoted U_{SLe}. The quantity πDLE_{r} is the rate at which mass is entrained from the liquid film into the control volume (gas core), where E_{r} is the entrainment rate per unit area. Under fully developed annular flow, the deposition rate of droplets from the gas core into the liquid film is equal to the entrainment rate and is also given by πDLE_{r}. The symbol τ_{fr} denotes the shear stress at the gas–liquid interface.

For annular flow, the liquid-holdup α_{L} is small—typically $\alpha_{\mathrm{L}} < 0.1$. Under these conditions, it is convenient approximate the gas velocity in the core with the superficial gas velocity, $U_{\mathrm{G}} \approx U_{\mathrm{SG}}$. Then, under the assumption that all droplets entrained from the surface of the liquid film are accelerated from the liquid film interface velocity U_{i} to the gas velocity in the core U_{SG} (Schadel et al., 1990), the momentum balance becomes:

$$\pi\frac{D^2}{4}L\frac{\mathrm{d}P}{\mathrm{d}x} + \pi DL\tau_{\mathrm{fr}} + \pi DLE_{\mathrm{r}}(U_{\mathrm{SG}} - U_{\mathrm{i}}) = 0. \tag{9}$$

The deposition of droplets from the gas core into the liquid film and the flux of droplets into the left-hand-side and out of the right-hand-side of the control volume do not contribute to the momentum balance since the velocity of these droplets does not change within the control surface (i.e. it remains U_{SG}). Solving for the pressure gradient, we obtain:

$$\frac{\mathrm{d}P}{\mathrm{d}x} = -\frac{4}{D}\tau_{\mathrm{fr}} - \frac{4}{D}E_{\mathrm{r}}(U_{\mathrm{SG}} - U_{\mathrm{i}}). \tag{10}$$

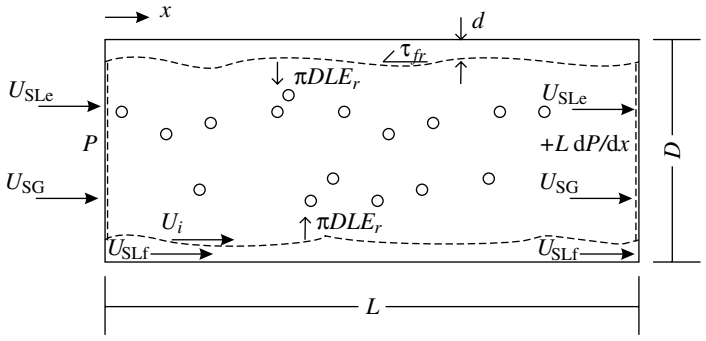

Fig. 1. Control volume of annular flow in a round pipe.

2.2. Interfacial friction

The first term on the right-hand-side of (10) is the pressure gradient due to interfacial friction. Wallis (1969) developed a model for the interfacial friction in terms of the thickness of the liquid film

$$\tau_{\mathrm{fr}} = 2f_{\mathrm{SG}}\left(1+\gamma\frac{d}{D}\right)\rho_{\mathrm{G}}(U_{\mathrm{SG}}-U_{\mathrm{i}})^2, \tag{11}$$

where d is the thickness of the liquid film, and γ is a parameter that characterizes the increase in the friction factor with film thickness.

For a flow of gas alone ($d = 0$, $U_{\mathrm{i}} = 0$), the above expression reduces to the expression for the pressure drop in a single-phase gas flow (4). The single-phase pressure drop was measured in the present experiments, but may also be estimated using an experimental correlation for the Fanning friction factor.

In the present experiment, most of the quantities in the above expression were not directly measured. Instead, they were estimated by means of experimental correlations.

For a flow with liquid present, the parameter γ is a proportionality constant between the thickness of the liquid film and the height of the waves on the surface of the film that act as roughness elements on a pipe wall. A higher γ indicates greater effective roughness and greater interfacial friction. Whalley and Hewitt (1978) recommend the expression:

$$\gamma = 24\left(\frac{\rho_{\mathrm{L}}}{\rho_{\mathrm{G}}}\right)^{1/3}. \tag{12}$$

For air–water flow at near-atmospheric pressures, γ is found in the range of 200–400. However, these values of γ account for the overall pressure gradient entirely via the interfacial shear term (11). When the component of the pressure gradient due to entrainment is accounted for (see Section 2.3), γ is lower. For the air–water data of Al-Sarkhi and Hanratty (2001a,b) we found $15 < \gamma < 105$, with γ increasing with the U_{SG}. For the present gas-condensate experiments, we found γ between 75 and 100. There was some dependence of γ on U_{SG} (see Section 4).

The velocity of the liquid at the gas–liquid interface is assumed to be approximately equal to the mean liquid velocity of the liquid film:

$$U_{\mathrm{i}} = \frac{U_{\mathrm{SLf}}}{\alpha_{\mathrm{Lf}}}, \tag{13}$$

where α_{Lf} is the liquid film holdup and is given by:

$$\alpha_{\mathrm{Lf}} = \frac{A_{\mathrm{Lf}}}{A}, \tag{14}$$

where A_{Lf} is the cross-sectional area of the pipe occupied by the liquid film, and A is the cross-sectional area of the pipe. U_{SLf} is the liquid film superficial velocity and is given by:

$$U_{\mathrm{SLf}} = U_{\mathrm{SL}}(1-E), \tag{15}$$

where E is the entrained fraction.

In the present experiment, the liquid holdup was measured as described in Section 3. Within the accuracy of the measurements, it remained unchanged for the flow with and without drag reducer. Knowing the liquid holdup, the liquid film holdup is estimated by assuming that there is no slip between the entrained droplets and the gas in the core (Oliemans, 1998):

$$\alpha_L = \alpha_{Lf} + (1 - \alpha_{Lf}) \frac{EU_{SL}}{U_{SG} + EU_{SL}}. \tag{16}$$

The entrained fraction, may be measured experimentally or estimated using an empirical correlation such as that proposed by Ishii and Mishima (1989):

$$E = \tanh\left(7.25 \times 10^{-7} We_l^{1.25} Re_{SLf}^{0.25}\right), \tag{17}$$

where We_L is the liquid Weber number and is given by:

$$We_L = We_{SG} \left(\frac{\Delta\rho}{\rho_G}\right)^{1/3}, \tag{18}$$

where $\Delta\rho = \rho_L - \rho_G$ is the density difference between the liquid and gas, and We_{SG} is the gas Weber number and is given by:

$$We_{SG} = \frac{\rho_G U_{SG}^2 D}{\sigma}, \tag{19}$$

where σ is the surface tension. The Reynolds number of the liquid film is defined as:

$$Re_{SLf} = Re_{SL}(1 - E), \tag{20}$$

where Re_{SL} is the superficial liquid Reynolds number, which is defined as:

$$Re_{SL} = \frac{\rho_L U_{SL} D}{\mu_L}, \tag{21}$$

where μ_L is the viscosity of the liquid.

2.3. Entrainment rate

The second term on the right-hand-side of (10) is the pressure gradient due to the entrainment of droplets from the annular liquid film into the gas core of the flow. The liquid that is entrained initially has a velocity of U_i, but upon entrainment the liquid droplets are assumed to be accelerated to the velocity of the gas core. The energy required to accelerate the droplets into the gas stream is dissipated upon the deposition of the droplets back into the liquid film. The energy dissipated due to this entrainment-deposition process manifests itself as an additional pressure gradient.

The entrainment rate was not measured in this experiment. Instead we used the correlation of Schadel et al. (1990):

$$E_r = U_{SG} \sqrt{\rho_L \rho_G} \frac{k\mu_L}{4} (Re_{SLf} - Re_{SLfc}), \tag{22}$$

where k is denoted the entrainment rate parameter, and Re_{SLfc} is the critical Reynolds number of the liquid film for the onset of entrainment. Even though their results were for a vertical flow, at

high superficial gas velocities we assume that it is a good description for horizontal flows as well. For an air water flow at near atmospheric conditions, Schadel et al. (1990) found $k \approx 0.00045$ m s/kg and $Re_{SLfc} \approx 200$ for a 25.4 mm pipe. For the air–water experiments of Al-Sarkhi and Hanratty (2001a,b), we found k in the range 0.0001–0.0006 m s/kg, with higher values for higher U_{SG} and lower values for lower pipe diameters. In the present gas-condensate experiments, we found values of k between 0.0006 and 0.0011 m s/kg. The exact values of k used were those that minimized the RMS error between the model and the pressure gradient data. There was some dependence of k on U_{SG} (see Section 4). Unpublished measurements (Vassiliadou, 1989) in our high-pressure gas-condensate flow facility found values of $Re_{SLfc} \approx 50$. However, since $Re_{SLf} \gg Re_{SLfc}$, the results are not sensitive to the choice of Re_{SLfc}.

Other authors have published experimental correlations for the entrainment rate in annular flows (e.g. Lopez de Bertodano et al., 2001; Pan and Hanratty, 2002) and these correlations may also be used.

2.4. Closure of drag-reduction model

Since the drag reducer reduces the roughness of the liquid film and suppresses entrainment from it, the drag reduction is modeled by modifying the parameters γ and k respectively in the interfacial friction and entrainment pressure gradient terms of the annular flow pressure gradient model (10).

In particular, we propose the following closure relationship:

$$\frac{\gamma}{\gamma_{DRA}} = R_\gamma \geqslant 1, \tag{23}$$

$$\frac{k}{k_{DRA}} = R_k \geqslant 1, \tag{24}$$

where γ_{DRA} and k_{DRA} are the respective values of the γ and k parameters with the addition of the DRA. The ratios R characterize the degree to which the DRA reduces the interfacial friction and entrainment rate parameters. The reduction in γ reflects the reduction of roughness of the gas–liquid interface while the reduction k reflects the decrease of the entrainment rate of liquid into gas stream.

The present understanding of the effect of DRAs in two-phase flows is not sufficiently well advanced to be able to relate the magnitudes of the ratios R_γ and R_k to the rheological properties of the polymers. Instead, the present experimental data was used to determine their values. We found that $R_\gamma = 2.6$ and $R_k = 3.0$ minimizes the root-mean-square (RMS) error between the measured drag reduction and the model. However, the accuracy of the drag reduction predictions is not sensitive to the precise values of R_γ or R_k. To simplify the closure, it is reasonable to take $R_\gamma = R_k = R$. Here, taking $R = 2.8$ gives good results as well.

While the particular values of γ, k, R_γ, and R_k used here are applicable to gas-condensate flow only, the approach to predicting drag reduction is applicable to any annular flow. In Section 4, the model is applied to the air–water drag reduction experiments of Al-Sarkhi and Hanratty (2001a,b). The values of the model parameters for air–water flows were determined and the model was found to be equally applicable.

3. Experiment

The present experiment was conducted in a high-pressure gas-condensate two-phase flow loop at Shell Research and Technology Centre—Amsterdam (SRTCA). The gas stream consisted of methane (CH_4) while the liquid stream was a condensate sample from a gas-condensate pipeline in the North Sea, with thermophysical properties close to that of decane ($C_{10}H_{22}$).

The drag-reducing agents used in the present experiments were high molecular weight poly-alpha-olefin polymers in a kerosene solvent—a so-called "gel" formulation. Al-Sarkhi and Hanratty (2001a) found that the drag reduction initially increases with increasing polymer concentration. However, beyond a certain threshold concentration—15 ppm (parts-per-million by mass in the liquid phase) in their experiments—no additional drag reduction is observed. In the present experiments, this concentration was found to be approximately 15 ppm as well. Three different poly-alpha-olefin molecules were used. The drag reduction was found to be insensitive to the choice of molecule as long as the concentration was at least 15 ppm.

In this study we were primarily interested in drag reduction in the region where the magnitude of drag reduction was independent of the DRA concentration. Consequently, all the data presented here are for drag reducer concentrations in excess of the 15 ppm threshold, such that the drag reductions represent the maximum multiphase drag reduction that can be achieved under the particular flow conditions being tested.

The flow loop is shown schematically in Fig. 2. The flow loop has a horizontal orientation, with an inner diameter of 19 mm and a length of approximately 120 m. The tubing was insulated and the temperature was regulated to 22 °C. The tubing is divided into 9 sections, each with a length of approximately 13 m. Each section was instrumented with a differential pressure transducer and a temperature transducer. The pressure gradient across each section was measured at a rate of 1 sample per second.

Both the condensate and gas are recirculated. The gas–liquid separation takes place in a vertical separator. The separator has a level indicator with a resolution of 0.5 cm such that the volume of liquid in the tubing can be measured and the liquid holdup calculated to within $\alpha_L = 0.01$. The

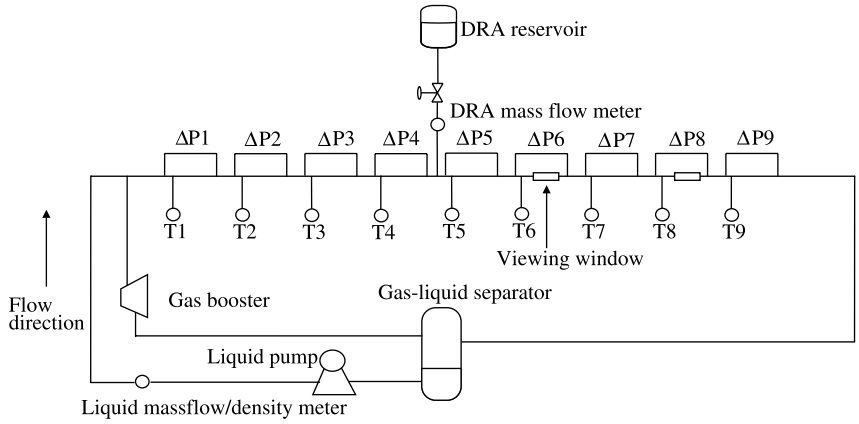

Fig. 2. Schematic of the high-pressure gas-condensate two-phase flow experiment.

addition of the DRA in the present experiments had no effect on the liquid holdup to within the resolution of the measurements.

The condensate was circulated using a positive displacement pump (gear pump) and injected into the inlet of the loop. The gas was circulated using three pneumatically driven positive displacement (piston) gas boosters (compressors) that are arranged in parallel. Depending on the gas velocity needed, either one, two, or all three gas boosters were used. The stroke rates of the boosters can be controlled individually and can vary from 5 to 20 strokes per minute.

The drag reducer was injected just upstream of section 5—i.e. approximately halfway through the loop. The experiments were conducted with an average absolute pressure of 11 bar in the pipe. Superficial gas velocities between 10.4 and 21.3 m/s, and superficial liquid velocities between 0.01 and 0.7 m/s were used. However, the annular flow regime only occurred for superficial gas velocities above approximately 8 m/s (see Section 4). The flow regime was observed at a viewing section located approximately 25 m downstream of the injection point. While it would be preferable to determine the flow regimes by means of differential pressure measurements rather than visually, the large pressure fluctuations introduced by the positive displacement gas compressors did not allow this.

The gas flow rates were measured by monitoring the stroke rate of the positive displacement gas boosters, which had a known stroke volume. The gas density was not measured but calculated by performing an isothermal flash calculation using the detailed composition data of the gas-condensate mixture. The condensate flow rate and density were measured directly using a coriolis mass flow meter. All other thermophysical properties of the gas and condensate (viscosity, surface tension) were estimated using the isothermal flash calculation. The experimental conditions are summarized in Table 1.

Since the DRA was injected upstream of section 5, the pressure gradients from sections 1 to 4 represent the pressure gradient without DRA while the pressure gradients from sections 5 to 9 represent the pressure gradient with DRA. Therefore, the pressure gradient measurements used to estimate the drag reductions are made simultaneously under essentially identical conditions. The changes in the gas density and velocity as a result of the pressure drop between the upstream and downstream sections were taken into account in calculating the friction factors and drag reduction via (2).

Table 1
Gas and liquid properties and experimental conditions

Property	Value	Units
Absolute pressure	10.9	bar
Temperature	22.0	°C
Liquid density	725	$kg\,m^{-3}$
Gas density	8.7	$kg\,m^{-3}$
Liquid viscosity	4.0×10^{-4}	$N\,s\,m^{-2}$
Gas viscosity	1.1×10^{-5}	$N\,s\,m^{-2}$
Surface tension	0.019	$N\,m^{-1}$
Gas molecular weight	18.6	
Gas compressibility	0.97	
Gas specific gravity	0.64	

Even though the DRA is injected upstream of section 5 and is recirculated, the pressure measurements showed that a single pass through the liquid pump completely sheared the polymer rendering it ineffective.

4. Results and discussion

Experiments were conducted at three superficial gas velocities ($U_{SG} = 10.4$, 16.6, and 21.3 m/s) in the annular flow regime. For each U_{SG}, the superficial liquid velocity was varied from 0.01 to 0.7 m/s. At the two highest U_{SG}, the U_{SL} that could be realized experimentally was limited by the liquid pump, which could not deliver high rates against the high differential pressures (approximately 4 bar). The superficial gas velocity of 21.3 m/s corresponds to the highest speed of the gas compressors.

The range of superficial gas velocities used here represents an F_{SG} range of 2.7–5.9. It corresponds to a U_{SG} range of approximately 30–80 m/s in an air–water experiment at near-atmospheric pressures in a pipe with the same diameter. In high-pressure gas-condensate flow, the transition between stratified and annular flow takes place at $F_{SG} \approx 2$ (Oliemans, 1998), which corresponds to a $U_{SG} = 8$ m/s in the present high-pressure gas-condensate experiment and $U_{SG} = 25$ m/s in an air–water flow in a pipe of the same diameter.

Fig. 3 shows the friction factor versus U_{SL} for the series of experiments with $U_{SG} = 10.4$, 16.6, and 21.3 m/s. The friction factors are normalized by the friction factor of the single-phase gas flow, f_{SG}. These were measured by running the experiment with no liquid, and are given in Table 2. The symbols are the experimental data. The solid lines are the predictions of the pressure

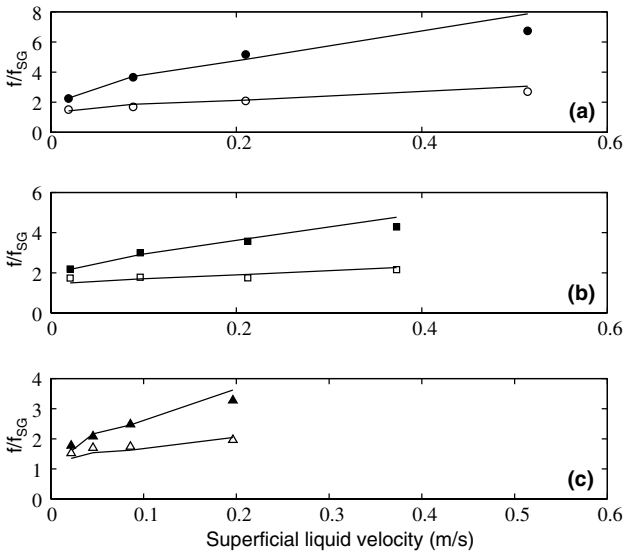

Fig. 3. Friction factor (f/f_{SG}) versus superficial liquid velocity (U_{SL}). (a) $U_{SG} = 10.4$ m/s, (b) $U_{SG} = 16.6$ m/s, (c) $U_{SG} = 21.3$ m/s. Symbols are the experimental data; filled symbols are for the flow with no DRA; hollow symbols are for the flow with DRA present. Lines are the pressure gradient model with and without DRA present.

Table 2
Results annular flow drag reduction experiments

U_{SG}	10.4	16.6	21.3	m/s
F_{SG}	2.7	4.5	5.9	
f_{SG}	0.0044	0.0034	0.0030	
$(dP/dx)_{SG}$	440	920	1400	Pa/m
γ	100	75	75	
k	0.0011	0.0006	0.0006	m s/kg
R_γ	2.6	2.6	2.6	
R_k	3.0	3.0	3.0	

gradient model (for the flow without DRA) and the drag reduction model (for the flow with DRA). The parameters used in the models were obtained by minimizing the RMS error between the experiments and the drag-reduction model and are given in Table 2. The model captures the pressure gradients both with and without DRA with an RMS error of approximately 5% of full scale.

Fig. 4 shows the drag reduction versus U_{SL} for each of the three superficial gas velocities. The symbols are the experimental data while the solid line is the drag reduction model. Note that the drag reduction was only calculated at discrete points corresponding to the superficial velocities where the experimental data exists—the line is drawn in order to aid the eye. The drag reduction model has an absolute RMS error of DR = 5%.

An important observation is that for a fixed superficial gas velocity (e.g. 10.4 m/s), the drag reduction increases with increasing superficial liquid velocity. However, beyond a certain threshold superficial liquid velocity (approximately 0.2 m/s), the drag reduction reaches a maximum. It essentially remains at this plateau level up to the highest U_{SL} used in the experiments.

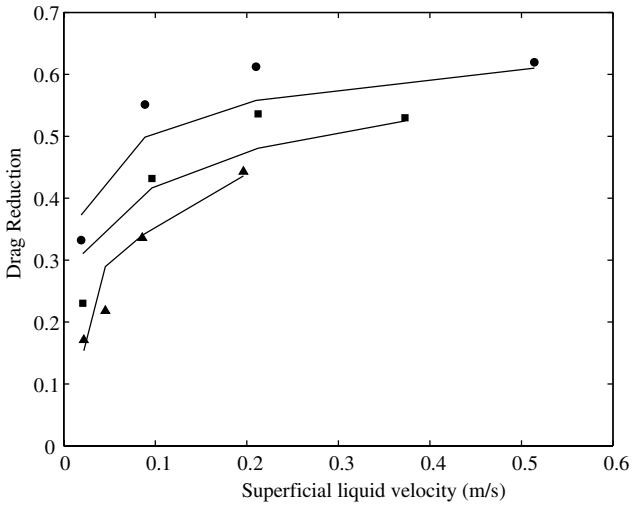

Fig. 4. Drag reduction (DR) versus superficial liquid velocity (U_{SL}). (●) $U_{SG} = 10.4$ m/s, (■) $U_{SG} = 16.6$ m/s, (▲) $U_{SG} = 21.3$ m/s. Symbols are the experimental data; lines are the drag reduction model.

The drag reduction model captures both the increase in DR versus U_{SL} at lower U_{SL} and the flattening out of the DR versus U_{SL} curve at higher U_{SL} (Fig. 4).

For a fixed superficial liquid velocity (e.g. 0.20 m/s) the higher the superficial gas velocity, the lower the drag reduction in annular flow. In particular, the maximum drag reduction decreases with increasing superficial gas velocity, going from 62% at $U_{SG} = 10.4$ m/s to 44% at $U_{SG} = 21.3$ m/s . The drag reduction model captures this behaviour. Even though the ratios are held fixed at $R_\gamma = 2.6$ and $R_k = 3.0$ respectively at each of the superficial velocities, the model yields the reduced maximum drag reduction with increasing U_{SG}.

We conclude that the present drag-reduction model captures the key qualitative and quantitative features of drag reduction in annular flow. The RMS error between the model and the data is approximately 5%. The main limitation in the applicability of the model is at very low U_{SL} (e.g. less than 0.02 m/s). Here, the experimental DR changes very quickly with U_{SL} and the model is not able to capture this.

In order to test the applicability of the present model to air–water flow, it was applied to the air–water drag reduction experiments of Al-Sarkhi and Hanratty (2001a) (9.53 cm pipe, $30 < U_{SG} < 43$ m/s) and Al-Sarkhi and Hanratty (2001b) (2.54 cm pipe, $24 < U_{SG} < 52$ m/s). This range of parameters represents an F_{SG} range of 1–4.

Fig. 5 shows the drag reductions versus the superficial liquid velocity for a superficial gas velocity of 36 m/s in the 9.53 cm pipe, and superficial gas velocities of 34 and 52 m/s in the 2.54 cm pipe. The symbols are the experimental data while the lines are the drag reduction model. The drag reduction was only calculated at discrete points corresponding to the superficial velocities where the experimental data exists; the lines are drawn in order to aid the eye. We found γ in the range 15–105, with γ increasing with U_{SG}, and decreasing with increasing pipe diameter. We found k in the range 0.0001–0.0006, with k increasing with U_{SG} and decreasing with increasing pipe diameter. The magnitude of the ratios R_γ and R_k were taken to be equal ($R_\gamma = R_k = R$), and were

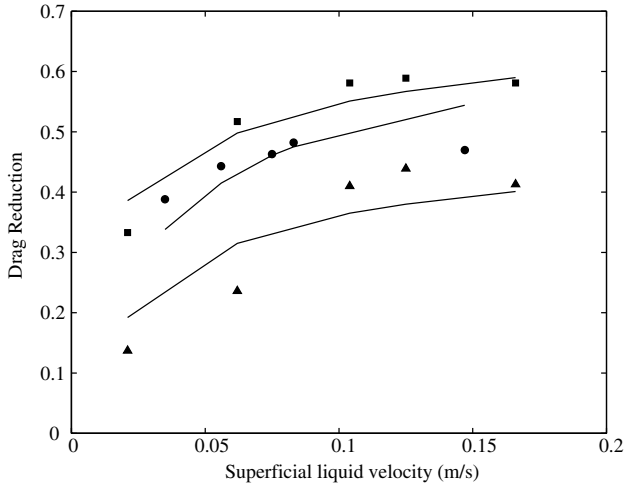

Fig. 5. Drag reduction (DR) versus superficial liquid velocity (U_{SL}) for the air–water data of Al-Sarkhi and Hanratty (2001a,b). (●) $U_{SG} = 36$ m/s, 9.53 cm pipe; $R_\gamma = R_k = 2.8$; (■) $U_{SG} = 34$ m/s, 2.54 cm pipe, $R_\gamma = R_k = 2.7$; (▲) $U_{SG} = 52$ m/s, 2.54 cm pipe, $R_\gamma = R_k = 1.9$. Symbols are the experimental data; lines are the drag reduction model.

found to be in the range 1.9–4.3. In general, R decreased with increasing superficial gas velocity with $R = 1.9$ corresponding to $U_{SG} = 52$ m/s and $R = 4.3$ corresponding to $U_{SG} = 24$ m/s. The magnitudes of the closure parameters R_γ and R_k are included in the caption. Again the model captures the key qualitative and quantitative features of drag reduction, including the effect of the diameter on the drag reduction. When applied to all the air–water data, the drag reduction model had an absolute RMS error of DR = 4%, slightly better than for application to the gas-condensate data.

The vast majority of multiphase pipelines in the field have densimetric Froude numbers within the range examined here; typically $F_{SG} < 3$. Under these circumstances, the results of the analysis of the gas-condensate and air–water drag reduction data suggests that taking the closure relationship as $R = 3$ will give reasonable estimates for the drag reduction. Applying $R = 3$ to the air–water experiments for all U_{SG} at both pipe diameters resulted in a RMS error of DR = 10% between the data and the model. Until data are available from field-scale drag reduction applications, using $R = 3$ is recommended.

In order to estimate the drag reduction, first apply the pressure gradient model (10) to obtain the pressure gradient in the flow without drag reducers. The values of γ and k should be within the ranges indicated here, with the magnitudes chosen such that the overall pressure gradient agrees with the laboratory measurements, field data, or another independent estimate of the pressure gradient. The results here suggest that as long as the overall pressure gradient is correct, the overall drag reduction will also be properly predicted. Only the distribution of the total drag reduction among the mechanisms may be improperly allocated.

4.1. Mechanisms of drag reduction

The measurements obtained in the experiments do not allow the direct determination of the distribution of the pressure gradient and the drag reduction between the two mechanisms—entrainment and interfacial friction. To do so would require the measurement of quantities such as the entrainment rate, the entrained fraction, and the film thickness. These quantities are difficult to obtain experimentally, and were not measured in the present experiment. However, the ability of the pressure gradient model and the drag reduction model to capture the quantitative and qualitative features of the experimental data, suggest that the model may be used to gain insight into the mechanisms of drag reduction. The results here are intended to be qualitative in nature and indicate trends rather than absolute numbers. Of course, any conclusions made using the model should be treated with caution until validated experimentally.

Fig. 6 shows the contribution of the interfacial friction and entrainment mechanisms to the total pressure gradient (versus superficial liquid velocity). The pressure gradients are normalized by the pressure gradient for the flow of dry gas alone $(dP/dx)_{SG}$, as indicated in Table 2. This is the same as plotting the friction factor for each mechanism normalized by the friction factor for single-phase gas flow.

According to (11), the pressure gradient due to interfacial friction is always at least as large as the pressure gradient due to the flow of dry gas alone. Fig. 6(a) indicates that at low U_{SG}, the interfacial friction contribution to the pressure gradient does not increase with increasing U_{SL}. This occurs since the $(U_{SG} - U_i)^2$ factor in (11) decreases with increasing U_{SL}, compensating for the increase in the $(1 + \gamma d/D)$ factor with U_{SL}. At higher U_{SG} (e.g. $U_{SG} = 21.3$ m/s), since U_{SG} is

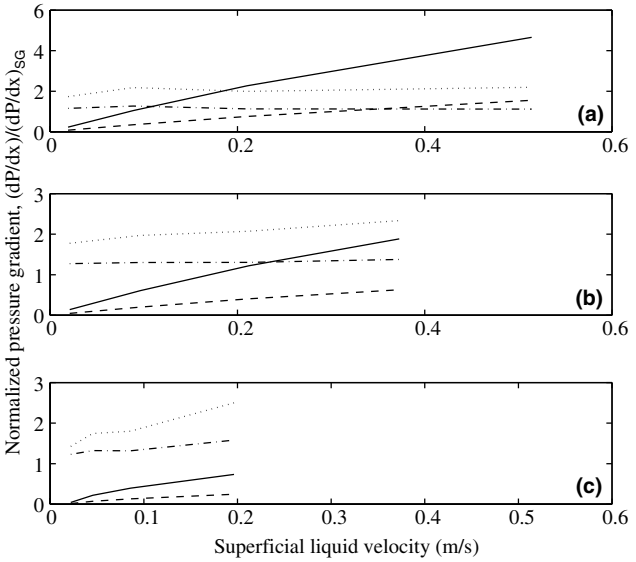

Fig. 6. Pressure gradient due to interfacial friction and liquid entrainment mechanisms versus superficial liquid velocity. Pressure gradients are normalized by the pressure gradient due to the flow of dry gas alone, $(\mathrm{d}P/\mathrm{d}x)/(\mathrm{d}P/\mathrm{d}x)_{\mathrm{SG}}$. (a) $U_{\mathrm{SG}} = 10.4$ m/s, (b) $U_{\mathrm{SG}} = 16.6$ m/s, (c) $U_{\mathrm{SG}} = 21.3$ m/s. (—) entrainment with no DRA; (- - -) entrainment with DRA; (· · ·) friction with no DRA; (· - · - ·) friction with DRA.

larger relative to U_{i} than at low U_{SG}, the relative decrease in the $(U_{\mathrm{SG}} - U_{\mathrm{i}})^2$ factor is lower and the contribution of the interfacial friction to the pressure gradient increases with increasing U_{SL}. The increase in interfacial friction with increasing U_{SL} for the flow with DRA is small for all U_{SG}.

The pressure gradient due to entrainment vanishes for low U_{SL}—i.e. U_{SL} that results in $Re_{\mathrm{SLf}} < Re_{\mathrm{SLfc}}$. Beyond Re_{SLfc}, the entrainment pressure gradient then increases approximately linearly with respect to U_{SL}. At low U_{SG}, since the interfacial friction contribution to the pressure gradient is relatively low (e.g. 1000 Pa/m for $U_{\mathrm{SG}} = 10.4$ m/s) and does not increase quickly with U_{SL}, the entrainment becomes the dominant pressure gradient mechanism beyond $U_{\mathrm{SL}} = 0.2$ m/s. However, at higher U_{SG}, as shown in Fig. 6(b) and (c), the interfacial friction is always the dominant mechanism.

The application of the drag-reduction model to the experimental data explains why the higher superficial gas velocities result in lower drag reductions in annular flow. Fig. 4 and Table 2 shows that the single-phase gas pressure gradient makes a greater fractional contribution to the total pressure gradient as U_{SG} increases. This component of the pressure gradient is always unaffected by the drag reducer—the effect of the DRA on the interfacial friction however is to make the interfacial friction pressure gradient curve approach the single-phase gas pressure gradient by a factor of R_γ. Thus, as U_{SG} increases, the model predicts a lower drag reduction. Fig. 4 shows that the model also captures this effect quantitatively.

Fig. 7 shows the fraction of the drag reduction due to the interfacial friction mechanism versus the superficial liquid velocity. For low U_{SL}, where there is little entrainment, the drag reduction is dominated by the interfacial friction term. However, the distribution of the drag reduction amongst the two mechanisms changes significantly with U_{SL} even though the ratios R_γ and R_k are

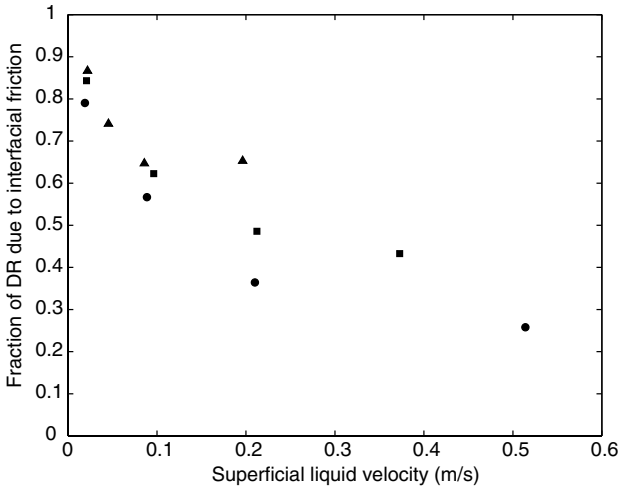

Fig. 7. Drag reduction due to interfacial friction mechanism versus superficial liquid velocity (U_{SL}). (●) $U_{SG} = 10.4$ m/s, (■) $U_{SG} = 16.6$ m/s, (▲) $U_{SG} = 21.3$ m/s.

approximately equal (2.6 and 3.0 respectively) and independent of U_{SL}. As suggested by Fig. 6, the entrainment pressure gradient generally increases more quickly with respect to U_{SL} than the interfacial friction pressure gradient. Thus, its reduction will also contribute relatively more to the drag reduction as U_{SL} increases. For low U_{SG} where the entrainment becomes the dominant contributor to the pressure gradient (low U_{SG}, high U_{SL}), the reduction of entrainment by the DRA becomes the dominant mechanism of drag reduction. Beyond $U_{SL} > 0.1$ m/s it contributes more than half of the overall drag reduction. However, as illustrated in Fig. 7, even where the interfacial friction is the dominant contributor to the pressure gradient (high U_{SG}), the reduction of entrainment can still be a significant mechanism of drag reduction.

As the absolute pressure in the pipe increases, the gas density increases. From (11) and (22) we find that $\tau_{fr} \sim \rho_G$ and $E_r \sim \sqrt{\rho_G}$ respectively. Therefore, as the absolute pressure increases the relative contribution of the frictional term to the overall pressure gradient increases. Consequently, the reduction of interfacial friction contributes an increasing fraction of the overall drag reduction as the absolute pressure increases.

As the pipe diameter increases, (11) and (22) indicate that $\tau_{fr} \sim D^{-1}$ and $E_r \sim D$ respectively. Therefore, as the diameter increases the reduction of interfacial friction accounts for a greater fraction of the overall drag reduction.

5. Summary and conclusions

We have presented experimental measurements of drag reduction a horizontal annular two-phase flow at experimental conditions close to those in gas-condensate pipelines in the field. The experiments were conducted in a high-pressure (10 bar) two-phase flow of methane (CH_4) and a condensate sample with thermophysical properties close to that of decane ($C_{10}H_{22}$).

Flow visualization showed that the injection of a DRA into an annular flow suppresses the liquid-film roughness and droplet entrainment from the liquid film into the gas core. Motivated by this, a mechanistic drag reduction model that quantifies the drag reduction by reducing the roughness (γ) and entrainment (k) parameters in the expression for the pressure gradient by a factor of R_γ and R_k respectively was developed. The proposed model does not consider the effect of the rheological properties of drag-reducing agents on the drag reduction. Instead, the experimental data were used to determine appropriate values of the model parameters γ and k, and the model closure relations for R_γ and R_k, for both gas-condensate and air–water flows.

We argue that the direct contribution of the turbulence in the liquid to the pressure gradient is negligible in annular flow and hence the drag reduction due to liquid turbulence suppression is also negligible. In this case, the reduction of frictional drag in an annular flow is primarily due to the modification of the flow regime or flow pattern and is a mechanism distinct from drag reduction in a single-phase flow.

In the annular flow regime, for a fixed superficial gas velocity, the magnitude of drag reduction increases with increasing superficial liquid velocity. Beyond a threshold U_{SL} (approximately $U_{SL} = 0.2$ m/s in this experiment) the DR reaches a maximum and remains there for increasing U_{SL} for all the U_{SL} examined (up to 0.7 m/s). For superficial gas velocities which result in an annular flow, the maximum DR decreases with increasing U_{SG}. Here, as the U_{SG} increased from 10.4 to 21.3 m/s the maximum DR decreased from 62% to 44%.

The comparison with the experimental data showed that the model captures the quantitative and qualitative features of the drag reduction in high-pressure gas-condensate annular flow and low-pressure air–water annular flow. The RMS error between the model and the experimental drag reduction, in both cases, was found to be approximately DR = 5%.

The analysis of the gas-condensate and air–water data suggests that under typical field conditions ($F_{SG} < 3$), using $R_\gamma = R_k = 3$, should result in drag reduction predictions within DR = $\pm$10%. This level of accuracy is sufficient to evaluate the technical and economic feasibility of the application of drag reducers to a particular multiphase pipeline. It is also sufficient to estimate the changes of gas and liquid flow rates, and pipeline pressures such that the impact of the drag reducers on the processing equipment downstream of the pipeline can be evaluated.

The drag-reduction model was used to gain insight into the relative contribution of the reduction of entrainment and interfacial friction to the overall drag reduction. From the examination of the air–water and gas-condensate drag reduction data in conjunction with the equations in Section 2, the distribution of drag reduction between the two mechanisms can be summarized as follows:

(1) For low superficial liquid velocities, the overall drag reduction is generally dominated by the reduction of interfacial friction.
(2) As the superficial liquid velocity increases, the reduction of entrainment accounts for a greater fraction of the overall drag reduction.
(3) As the superficial gas velocity increases, the reduction of interfacial friction accounts for a greater fraction of the overall drag reduction.
(4) As the pipe diameter increases, the reduction of entrainment accounts for a greater fraction of the overall drag reduction.
(5) As the absolute pressure increases (i.e. ρ_G increases), the reduction of interfacial friction accounts for a greater fraction of the overall drag reduction.

Acknowledgements

The authors would like to thank Ulfert Klomp and Henk Keemink of Shell Research and Technology Centre Amsterdam (SRTCA) for the use of the high-pressure gas-condensate flow-loop and for all of their help in conducting the drag reduction experiments.

References

Al-Sarkhi, A., Hanratty, T.J., 2001a. Effect of drag-reducing polymers on annular gas–liquid flow in a horizontal pipe. Int. J. Multiphase Flow 27, 1151–1162.

Al-Sarkhi, A., Hanratty, T.J., 2001b. Effect of pipe diameter on the performance of drag-reducing polymers in annular gas–liquid flows. Trans. IChemE, Part A 79.

Bachman, H.E., Shih, C.K., 1994. Method of suppressing mist formation from oil-containing functional fluids. US Patent 5,329,055.

Daas, M., Kang, C., Jepson, W.P., 2000. Quantitative analysis of drag reduction in horizontal slug flow. Society of Petroleum Engineers, SPE 62944.

Fernandes, R.L.J., 2003. Multiphase drag reduction in horizontal flows. In: 11th International Conference on MULTIPHASE 03, pp. 359–372.

Ishii, M., Mishima, K., 1989. Droplet entrainment correlation in annular two-phase flow. Int. J. Heat Mass Transfer 32, 1835–1846.

Kang, C., Jepson, W.P., 1999. Multiphase flow conditioning using drag-reducing agents. Society of Petroleum Engineers, SPE 56569.

Kang, C., Jepson, W.P., 2000. Effect of drag-reducing agents in multiphase, oil/gas horizontal flow. Society of Petroleum Engineers, SPE 58976.

Khatib, Z.I., 1998. Prevention of shearing of hydrocarbon droplets to aerosol sizes. US Patent 5,849,983.

Lopez de Bertodano, M.A., Assad, A., Beus, S.G., 2001. Experiments for entrainment rate of droplets in the annular regime. Int. J. Multiphase Flow 27, 685–699.

Manfield, P.D., Lawrence, C.J., Hewitt, G.F., 1999. Drag reduction with additives in multiphase flow: a literature survey. Multiphase Sci. Technol. 11, 197–221.

Miesen, R.H.M., 1994. Internal communication.

Oliemans, R.V.A., 1998. Applied Multiphase Flows. Delft University of Technology, Delft.

Pan, L., Hanratty, T.J., 2002. Correlation of entrainment for annular flow in horizontal pipes. Int. J. Multiphase Flow 28, 385–408.

Schadel, S.A., Leman, G.W., Binder, J.L., Hanratty, T.J., 1990. Rates of atomization and deposition in vertical annular flow. Int. J. Multiphase Flow 16, 363–374.

Sylvester, N.D., Brill, J.P., 1976. Drag-reduction in two-phase annular mist flow of air and water. AIChE J. 22, 615–617.

Vassiliadou, E.A., 1989. Internal communication.

Wallis, G.B., 1969. One-Dimensional Two-Phase Flow. McGraw-Hill, New York.

Whalley, P.B., Hewitt, G.F., 1978. The correlation of liquid entrainment fraction and entrainment rate in annular two-phase flow. Tech. Rep. AERE-R 9187, UKAEA, Harwell, Oxon.

Wilkens, R.J., Glassmeyer, S.R., Rosebrock, G.J., Storage, K.M., Storage, T.M., 2003. Surfactant use for slug flow pattern suppression in a horizontal pipe. No. GL-024-US. In: Proceedings of the 8th International Symposium on Gas–Liquid Flows: ASME/JSME Joint Fluids Engineering Division Summer Meeting.